Inorg. Chem. **2004**, *43*, 4254–4261

Crystal Growth, Observation, and Characterization of the Low-Temperature Structure of the Fluorite-Related Ruthenates: Sm_3RuO_7 and Eu_3RuO_7

William R. Gemmill, Mark D. Smith, and Hans-Conrad zur Loye*

Department of Chemistry and Biochemistry, University of South Carolina, Columbia, South Carolina 29208

Received March 8, 2004

The compounds Sm_3RuO_7 and Eu_3RuO_7 were grown as single crystals from molten hydroxide fluxes. They crystallize in the orthorhombic space group *Cmcm* and are part of a well-known family of fluorite-related oxides of stoichiometry Ln_3MO_7. This structure contains rare earth cations in two different coordination environments, 8-fold pseudocubic and 7-fold pentagonal bipyramidal, and contains Ru(V) cations that are octahedrally coordinated. The RuO_6 octahedra are trans vertex-sharing to yield chains oriented along the *c*-axis. Upon cooling, single crystals of Sm_3RuO_7 and Eu_3RuO_7 undergo a structural transition at 190 and 280 K, respectively, from space group *Cmcm* to $P2_1nb$. The structure transition results in a loss of lattice centering, a doubling of the *b*-axis, a distortion of the vertex-shared Ru–O chains, and a reduction in the coordination of one of the rare earth cations from 8-fold to 7-fold. Accompanying this structural transition are anomalies in the magnetic susceptibility at about 190 and 280 K for Sm_3RuO_7 and Eu_3RuO_7, respectively. The structures of these low-temperature phases of Ln_3RuO_7 have been determined for the first time and are described.

Introduction

High-temperature solutions, including alkali and alkaline earth carbonates, halides, peroxides, and hydroxides,[1] are an effective medium in which to grow oxide single crystals that could contain nearly any element of the periodic table.[2] Of these diverse solvent systems, hydroxides are particularly well suited for the preparation of complex metal oxides containing elements in unusual or high oxidation states.[3,4] The acid−base chemistry of hydroxide fluxes, described by the Lux−Flood acid−base definition,[5,6] allows for a wide range of species to be present in solution, an essential prerequisite for their incorporation into single crystals.

It is known that molten hydroxides are an excellent solvent of crystallization for lanthanide-containing oxides,[7,8] where the solubility of the lanthanides is dictated by the acid−base properties of the melt. Specifically, the water content of the melt must be controlled to enable the dissolution of the lanthanide oxides (Ln_2O_3's),[5,6,9] which are only soluble in acidic wet melts.[7] We have recently shown that such wet melts are one route for the growth of oxide single crystals containing both lanthanide and platinum group metals.[10] As part of our systematic investigation of the Ln−Ru−O phase space, we prepared single crystals of Ln_3RuO_7 (Ln = Sm, Eu), members of a well-known family of fluorite-related oxides of stoichiometry Ln_3MO_7.

The family of compounds of the general formula Ln_3MO_7, in which Ln is a lanthanide and M is a pentavalent metal cation, was first reported by Allpress and Rossell in 1979 and was described as having an orthorhombic, fluorite-related structure.[11] Since then, many compositions have been prepared and investigated, including Ln_3MO_7 (Ln = La, Pr, Nd; M = Nb, Ta, Sb),[11−14] Ln_3RuO_7 (Ln = La, Pr, Nd, Sm,

* To whom correspondence should be addressed. E-mail: zurloye@sc.edu.

(1) Stitzer, K. E.; Darriet, J.; zur Loye, H.-C. *Curr. Opin. Solid State Mater. Sci.* **2001**, *5*, 535.
(2) Elwell, D.; Scheel, H. J. *Crystal Growth from High-Temperature Solutions*; Academic Press: New York, 1975.
(3) Reisner, B. A.; Stacy, A. M. *J. Am. Chem. Soc.* **1998**, *120*, 9682.
(4) Stitzer, K. E.; Smith, M. D.; Gemmill, W. R.; zur Loye, H.-C. *J. Am. Chem. Soc.* **2002**, *124*, 13877.
(5) Lux, H. *Z. Elektrochem.* **1939**, *45*, 303.
(6) Flood, H.; Forland, T. *Acta Chem. Scand.* **1947**, *1*, 592.
(7) Keller, S. W.; Carlson, V. A.; Sanford, D.; Stenzer, F.; Stacy, A. M.; Kwei, G. H.; Alario-Franco, M. *J. Am. Chem. Soc.* **1994**, *116*, 8070.
(8) Luce, J. L.; Stacy, A. M. *Chem. Mater.* **1997**, *9*, 1508.
(9) Goret, J. *Bull. Soc. Chim.* **1964**, 1074.
(10) Davis, M. J.; Smith, M. D.; zur Loye, H.-C. *Inorg. Chem.* **2003**, *42*, 6980.
(11) Allpress, J. G.; Rossell, H. J. *J. Solid State Chem.* **1979**, *27*, 105.
(12) Rossell, H. J. *J. Solid State Chem.* **1979**, *27*, 287.

10.1021/ic049700l CCC: $27.50
Published on Web 06/12/2004

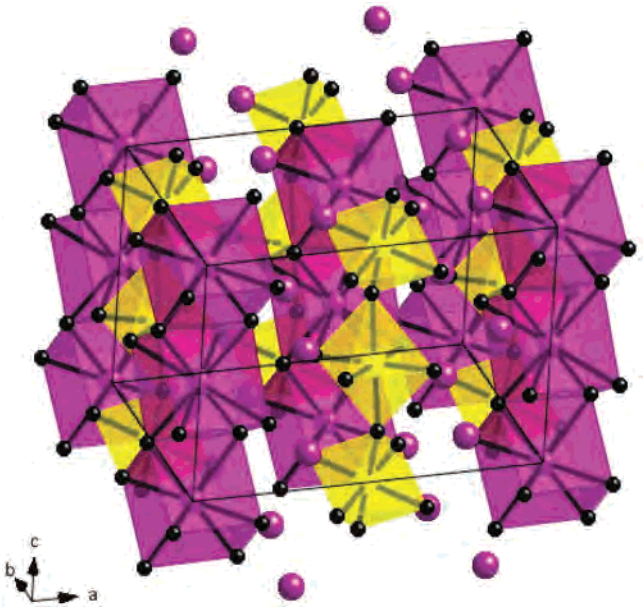

Figure 1. Crystal structure of the high-temperature *Cmcm* structure of Ln_3RuO_7 (Ln = Sm, Eu), emphasizing the chains of trans vertex-sharing RuO_6 octahedra (yellow) which are edge-shared to chains of $Ln(1)O_8$ pseudocubes (violet) along the *c*-axis. The violet spheres are the $Ln(2)^{3+}$ cations.

Eu, Gd),[15−19] Ln_3ReO_7 (Ln = La, Pr, Nd, Sm, Gd, Tb, Dy),[20−22] Ln_3OsO_7 (Ln = La, Pr, Nd, Sm),[23,24] and Ln_3IrO_7 (Ln = Pr, Nd, Sm, Eu).[25,26] The structure of these compounds is well described in the orthorhombic space group *Cmcm* and features chains of trans vertex-sharing MO_6 octahedra that are oriented along the *c*-axis and that are tilted in the *bc*-plane. In this structure, the lanthanide cations are located in two different coordination environments, 8-fold pseudocubic and 7-fold pentagonal bipyramidal, and the Ru(V) cations are located in octahedral coordination (Figure 1). To date, there are only two known members of the Ln_3MO_7 family that do not crystallize in the *Cmcm* space group: Ln_3NbO_7 and Ln_3MoO_7, which crystallize in the space groups *Pnma* and $P2_12_12_1$, respectively.[14,27]

Recently, detailed magnetic and thermal investigations were reported for the ruthenium- and iridium-containing members of the Ln_3MO_7 family, which provided evidence for the existence of low-temperature structural phase transitions and showed that the transition temperature is a function of the specific lanthanide ion in the Ln_3MO_7 (M = Ir, Ru) oxides.[26−30] One of the ruthenates that undergoes this structure transition, Nd_3RuO_7, was recently investigated by low-temperature neutron diffraction and reported to undergo an orthorhombic (space group *Cmcm*) to monoclinic (space group $P2_1/m$) structural phase transition at 130 K.[30] Other ruthenate members of this family also undergo structure transitions; however, in those cases, only the high-temperature *Cmcm* structure has been determined. In the latter cases, the growth of single crystals would be extremely beneficial for structural investigations, as low-temperature single-crystal X-ray diffraction experiments could be performed. In the Ln_3MO_7 family of oxides, to the best of our knowledge, only two members, Sm_3ReO_7[21] and La_3NbO_7,[14] have been prepared as single crystals.

To further investigate the structure transitions and to determine the low-temperature structures for some of the ruthenate members of this family, we have grown single crystals of the compounds Ln_3RuO_7 (Ln = Sm, Eu). Herein, we report the conditions used to grow these crystals and the single-crystal structure determination of the low- and the high-temperature phases.

Experimental Section

Crystal Growth. For both Sm_3RuO_7 and Eu_3RuO_7, 1.00 mmol of RuO_2 [synthesized from heating Ru powder (Engelhard, 99.5%) in air for 24 h], 1.5 mmol of Ln_2O_3 (Alfa Aesar, REacton, 99.9%), a 10-fold mass excess of NaOH (Fisher, ACS reagent), and 0.5 g of H_2O were placed into a silver tube that had been flame-sealed on one end. The silver tube was then crimped shut on the other end, placed into a box furnace, and heated to the reaction temperature of 600 °C at 10 °C/min. The reaction was held at temperature for 12 h and then cooled to room temperature by turning off the furnace. The flux was dissolved with water aided by the use of sonication, after which the crystals were manually isolated.

Single-Crystal X-ray Diffraction. Evaluation of the X-ray diffraction patterns, unit cell indexing, and intensity data measurements for both compounds were performed on a Bruker SMART APEX CCD-based diffractometer employing Mo Kα radiation (λ = 0.710 73 Å).[31] Raw area detector intensity data frames were integrated and corrected for Lorentz-polarization effects with SAINT-PLUS.[31] Absorption corrections based on the multiple measurement of equivalent reflections were applied to the data sets with SADABS.[31] Direct methods structure solution, difference Fourier calculations, and full-matrix least-squares refinement against F^2 were performed with SHELXTL.[32] Suitable crystals were

(13) Rossell, H. J. *J. Solid State Chem.* **1979**, *27*, 115.
(14) Kahn-Harari, A.; Mazerolles, L.; Michel, D.; Robert, F. *J. Solid State Chem.* **1995**, *116*, 103.
(15) van Berkel, F. P. F.; IJdo, D. J. W. *Mater. Res. Bull.* **1986**, *21*, 1103.
(16) Khalifah, P.; Huang, Q.; Lynn, J. W.; Erwin, R. W.; Cava, R. J. *Mater. Res. Bull.* **2000**, *35*, 1.
(17) Khalifah, P.; Erwin, R. W.; Lynn, J. W.; Huang, Q.; Batlogg, B.; Cava, R. J. *Phys. Rev. B: Condens. Matter Mater. Phys.* **1999**, *60*, 9573.
(18) Wiss, F.; Raju, N. P.; Wills, A. S.; Greedan, J. E. *Int. J. Inorg. Mater.* **2000**, *2*, 53.
(19) Bontchev, R. P.; Jacobson, A. J.; Gospodinov, M. M.; Skumryev, V.; Popov, V. N.; Lorenz, B.; Meng, R. L.; Litvinchuk, A. P.; Iliev, M. N. *Phys. Rev. B: Condens. Matter Mater. Phys.* **2000**, *62*, 12235.
(20) Lam, R.; Langet, T.; Greedan, J. E. *J. Solid State Chem.* **2003**, *171*, 317.
(21) Wltschek, G.; Paulus, H.; Svoboda, I.; Ehrenberg, H.; Fuess, H. *J. Solid State Chem.* **1996**, *125*, 1.
(22) Hinatsu, Y.; Wakeshima, M.; Kawabuchi, N.; Taira, N. *J. Alloys Compd.* **2004**, *374*, 79.
(23) Plaisier, J. R.; Drost, R. J.; IJdo, D. J. W. *J. Solid State Chem.* **2002**, *169*, 189.
(24) Lam, R.; Wiss, F.; Greedan, J. E. *J. Solid State Chem.* **2002**, *167*, 182.
(25) Vente, J. F.; IJdo, D. J. W. *Mater. Res. Bull.* **1991**, *26*, 1255.
(26) Nishimine, H.; Wakeshima, M.; Hinatsu, Y. *J. Solid State Chem.* **2004**, *177*, 739.
(27) Greedan, J. E.; Raju, N. P.; Wegner, A.; Gougeon, P.; Padiou, J. *J. Solid State Chem.* **1997**, *129*, 320.
(28) Harada, D.; Hinatsu, Y. *J. Solid State Chem.* **2001**, *158*, 245.
(29) Harada, D.; Hinatsu, Y. *J. Solid State Chem.* **2002**, *164*, 163.
(30) Harada, D.; Hinatsu, Y.; Ishii, Y. *J. Phys.: Condens. Matter* **2001**, *13*, 10825.
(31) *SMART* version 5.625, S. V., and *SADABS* version 2.05; Bruker Analytical X-ray Systems, Inc.: Madison, WI, 2001.
(32) Sheldrick, G. M. *SHELXTL*; Bruker Analytical X-ray Systems, Inc., Madison, WI, 1997.

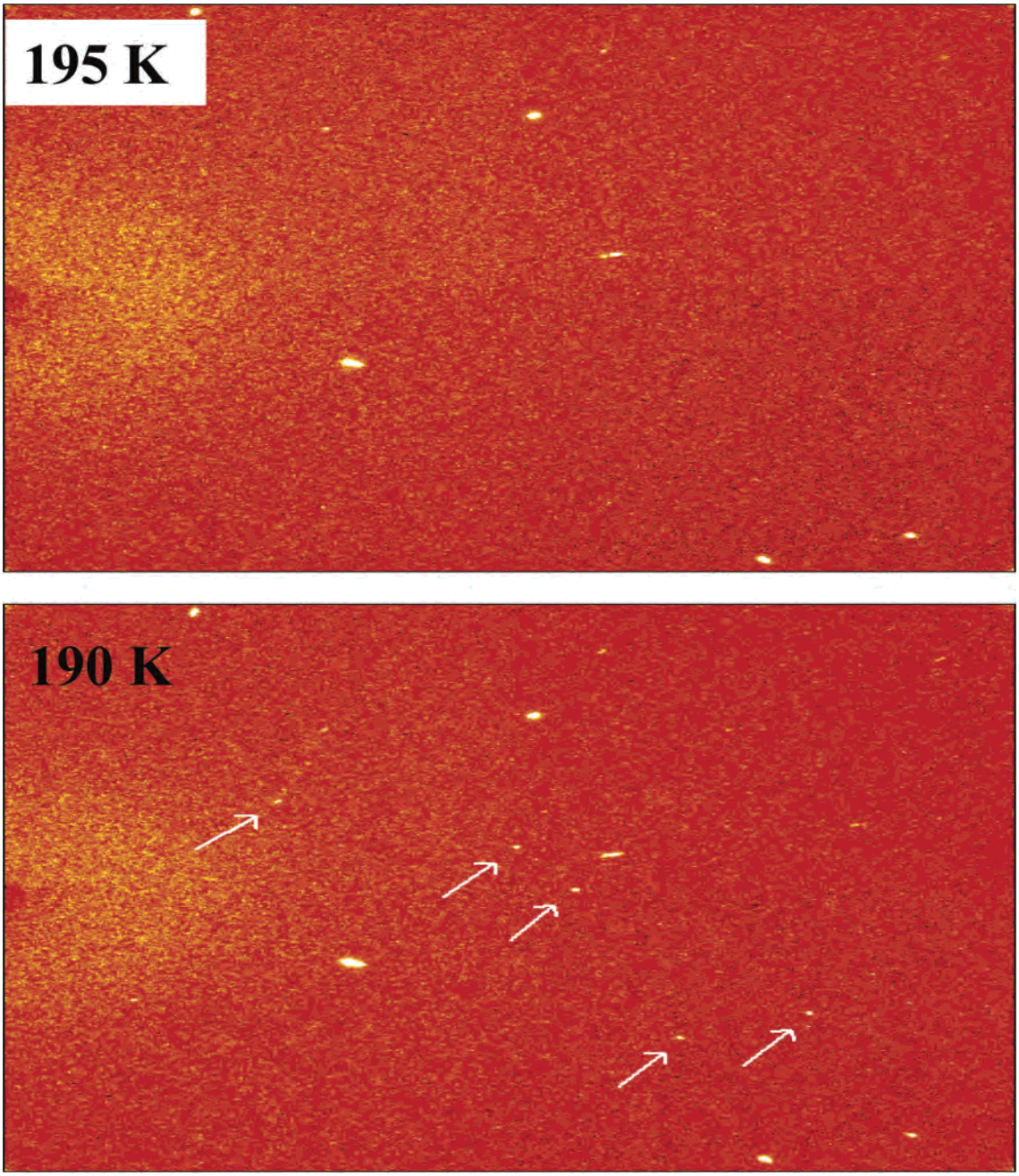

Figure 2. Appearance of additional spots in the diffraction pattern for Sm_3RuO_7 (indicated by arrows, lower frame) corresponding to the onset of the *Cmcm* → $P2_1nb$ structural transition at approximately 190 K. Both exposures were taken with the crystal in the same orientation.

selected and epoxied onto thin glass fibers for the room-temperature measurement and frozen onto the tip of a glass fiber for the low-temperature measurements. The same crystal of each compound was used for both the high- and low-temperature data collections.

High-Temperature Structures. Careful examination of long-exposure area detector frames taken above the transition temperature (Figure 2) from single crystals of Sm_3RuO_7 and Eu_3RuO_7 showed no evidence for a unit cell other than the anticipated *C*-centered orthorhombic cell with $a \approx 10.7$ Å, $b \approx 7.3$ Å, and $c \approx 7.4$ Å. Highly redundant intensity data sets were collected at 220 K for Sm_3RuO_7 and at 294 K for Eu_3RuO_7. After raw data processing, refinement in the space group *Cmcm* using coordinates from isostructural Ln_3MO_7 phases proceeded without difficulty in each case.[21] All atoms were refined with anisotropic displacement parameters. Refinement of the site occupation factors for the metal atoms showed no deviation from full occupancy in either case. Final refinement statistics for the room-temperature data sets are compiled in Table 1.

Low-Temperature Structures. Upon cooling the crystals used for the high-temperature measurements below approximately 190 K for Sm_3RuO_7 and 280 K for Eu_3RuO_7, additional diffraction spots appeared in the area detector frames (Figure 2). Though weak, all additional diffraction peaks could be indexed to a primitive orthorhombic cell with $a \approx 10.7$ Å, $b \approx 14.6$ Å, and $c \approx 7.4$ Å, corresponding to a doubling of the *b*-axis of the high-temperature *Cmcm* cell and a loss of lattice centering. Data were collected at 150 K for both compounds, using long exposures (45 s per frame) to account for the weaker superstructure reflections. Systematic absences in the intensity data for each compound indicated the space groups *Pmnb* or $P2_1nb$, the latter being the acentric counterpart of

Table 1. Crystallographic Data and Structure Refinement for the High-Temperature Structure of Sm_3RuO_7 and Eu_3RuO_7

empirical formula	Sm_3RuO_7	Eu_3RuO_7
fw (g/mol)	664.12	668.95
temp (K)	220(2)	294(2)
wavelength (Å)	0.710 73	0.710 73
cryst syst	orthorhombic	orthorhombic
space group	*Cmcm*	*Cmcm*
unit cell dimensions	$a = 10.7492(3)$ Å, $\alpha = 90°$	$a = 10.6926(5)$ Å, $\alpha = 90°$
	$b = 7.3125(2)$ Å, $\beta = 90°$	$b = 7.3078(3)$ Å, $\beta = 90°$
	$c = 7.4387(3)$ Å, $\gamma = 90°$	$c = 7.4107(3)$ Å, $\gamma = 90°$
vol (Å^3)	584.71(3)	579.14(4)
Z	4	4
density (Mg/m^3)	7.544	7.672
abs coeff (mm^{-1})	32.199	34.581
reflns collected	4695	3971
indep reflns	715 [R(int) = 0.0270]	678 [R(int) = 0.0429]
absorption correction	semiempirical from equivalents	semiempirical from equivalents
data/restraints/params	715/0/35	678/0/35
GOF on F^2	1.124	1.176
final R indices [$I > 2\sigma(I)$]	R1 = 0.0191, wR2 = 0.0482	R1 = 0.0264, wR2 = 0.0546
R indices (all data)	R1 = 0.0200, wR2 = 0.0487	R1 = 0.0300, wR2 = 0.0559
extinction coefficient	0.004 44(17)	0.0056(2)
largest diff peak and hole (e·Å^{-3})	1.767 and −1.576	3.115 and −2.604

the former. (Note: Space groups *Pmnb* and $P2_1nb$ are nonstandard settings of *Pnma* and $Pna2_1$, respectively, and were chosen here to facilitate comparison with the *Cmcm* structures; i.e., the Ru—O polyhedral chains run along the same axis in both structures, vide infra.) An initial structure solution was obtained in the centrosymmetric *Pmnb* but resulted in several physically unreasonable (nonpositive definite) displacement parameters for the metal atoms, high (>10%) *R*-factors, and large residual electron densities (>15 e$^-$/Å^3). Solution and refinement in $P2_1nb$ yielded reasonable displacement parameters and satisfactory refinements in both cases. For Sm_3RuO_7, the direct methods solution located 2 independent Ru positions and 6 independent Sm positions. There were 14 independent oxygen atom positions locatedin subsequent difference maps. The 8 metal atoms were refined anisotropically; the oxygen atoms could only be refined isotropically. At this stage of the refinement, the absolute structure (Flack) parameter was ca. 0.5, indicating a perfect inversion twin. Such twinning is required in a centric-to-acentric structural transition where the loss of a symmetry center leaves a polar axis (the *a*-axis in this case) with a statistically equal probability to orient in either of two directions. The inversion twin operator was included in the final refinement cycles with the twin fraction fixed at 0.5.

Eu_3RuO_7 was refined analogously in $P2_1nb$ using the atomic coordinates from Sm_3RuO_7, with the exception that only 3 metal atoms [Eu(1), Eu(2), and Eu(4)] were refined anisotropically. This is most likely due to lower crystal quality, a fact that is also evident in the refinement statistics of the high-temperature structure (Table 1). Final refinement statistics for the low-temperature data sets are compiled in Table 4.

Scanning Electron Microscopy. Environmental scanning electron micrographs (ESEMs) of several single crystals were obtained using an FEI Quanta 200 ESEM instrument utilized in the low-vacuum mode. ESEM images of the representative crystals of Ln_3RuO_7 (Ln = Sm, Eu) are shown in Figure 3a,b, respectively. Energy dispersive spectroscopy (EDS) also verified the presence of samarium, ruthenium, and oxygen in Sm_3RuO_7 and europium, ruthenium, and oxygen in Eu_3RuO_7. Furthermore, within the detection limit of the instrument, no other extraneous elements were detected.

Magnetic Susceptibility. The magnetic susceptibility of the compounds Ln_3RuO_7 (Ln = Sm, Eu) was measured using a Quantum Design MPMS XL SQUID magnetometer. For the magnetic measurements, loose crystals of each ruthenate were placed into a gelatin capsule, which was placed inside a plastic straw. Samples were measured under both zero-field-cooled (ZFC) and field-cooled (FC) conditions. For Sm_3RuO_7 and Eu_3RuO_7, the magnetization was measured in the temperature ranges 2−300 and 2−350 K, respectively. Susceptibility measurements were carried out in an applied field of 10 kG. The very small diamagnetic contribution of the gelatin capsule containing the sample had a negligible contribution to the overall magnetization, which was dominated by the sample signal.

Results and Discussion

Room-Temperature Structures. Small, black prismatic crystals, averaging 0.1−0.2 mm in length, were isolated from a molten hydroxide flux and used for single-crystal X-ray diffraction measurements. Representative SEM images of Ln_3RuO_7 (Ln = Sm, Eu) are shown in Figure 3a,b, respectively, where the interpenetration twinning evident in these images underscores the difficulty encountered in selecting a genuinely single crystal for the diffraction measurements.

An analysis of the single-crystal diffraction data confirmed that both Sm_3RuO_7 and Eu_3RuO_7 crystallize in the structure and space group (*Cmcm*) reported for the Ln_3MO_7 family of oxides. This high-temperature orthorhombic *Cmcm* structure, Figure 1, features chains of trans vertex-sharing RuO_6 octahedra that run along the *c*-axis. One-third of the lanthanide cations, Ln(1), are in a distorted cubic 8-fold coordination environment, forming chains of edge-sharing $Ln(1)O_8$ pseudocubes that concomitantly share edges with the chains of RuO_6 octahedra, generating slabs that lie parallel to the *bc*-plane. The remaining lanthanide cations, Ln(2), are located between these layers, where they exist in a 7-fold distorted pentagonal bipyramidal coordination environment.

The Ru—O bond distances are in the ranges 1.942(3)−1.9584(17) and 1.939(4)−1.949(3) Å for Sm_3RuO_7 and Eu_3RuO_7, respectively. These values agree well with the previously reported powder X-ray diffraction Rietveld refinements for these two compounds as well as with Ru—O bond lengths reported for other Ln_3RuO_7 oxides of this structure type.[28−30] All crystallographic data and atomic positions for the high-temperature structures are listed in Tables 1 and 2, respectively. Selected interatomic distances and angles are listed in Table 3.

Low-Temperature Structures. Recently, Hinatsu et al. reported on the magnetic and thermal properties of the series Ln_3RuO_7 (Ln = Pr, Nd, Sm, Eu, Gd),[28−30] in which they observed anomalies in both the magnetic and thermal data that strongly suggested the existence of a structural transition in each of the above oxides. They were able to confirm the existence of such a structural transition at 130 K in Nd_3RuO_7, and they solved the low-temperature structure in the

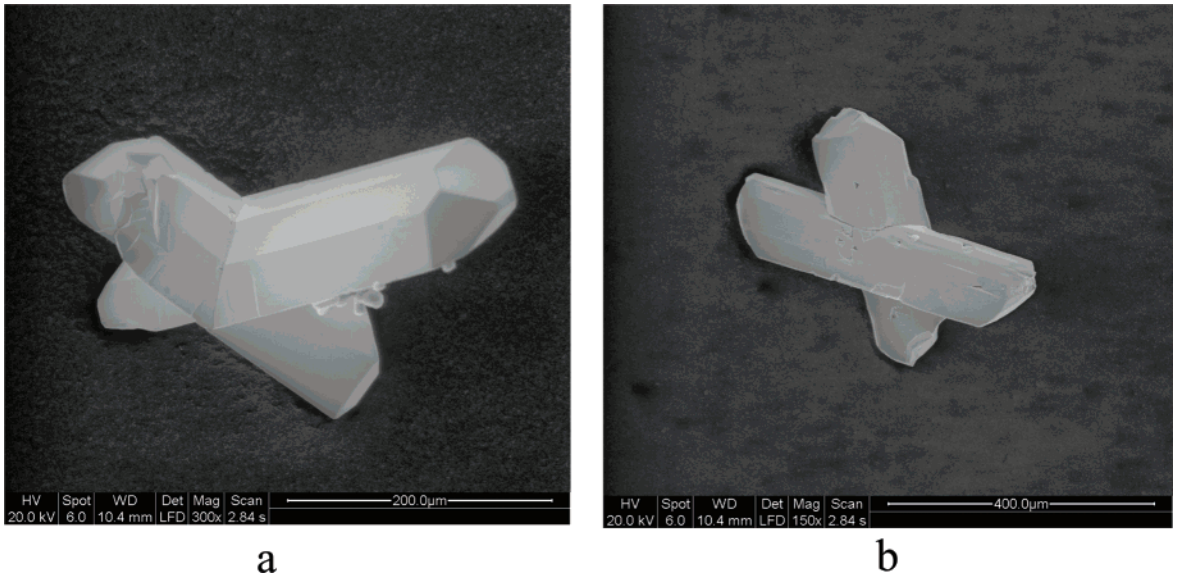

Figure 3. ESEM images of flux-grown crystals of (a) Sm_3RuO_7 and (b) Eu_3RuO_7 emphasizing the interpenetration growth morphology.

Table 2. Atomic Coordinates and Equivalent Isotropic Parameters for the High-Temperature Structure of Sm_3RuO_7 and Eu_3RuO_7

Sm_3RuO_7	*x*	*y*	*z*	U_{eq} (Å^2)
Sm(1)	0	0	0	0.010(1)
Sm(2)	0.2233(1)	0.3057(1)	1/4	0.005(1)
Ru	0	1/2	0	0.003(1)
O(1)	0.1266(3)	0.3149(4)	−0.0402(4)	0.012(1)
O(2)	0.1309(4)	0.0275(5)	1/4	0.007(1)
O(3)	0	0.4160(7)	1/4	0.006 (1)
Eu_3RuO_7	*x*	*y*	*z*	U_{eq} (Å^2)
Eu(1)	0	0	0	0.014(1)
Eu(2)	0.2238(1)	0.3045(1)	1/4	0.007(1)
Ru	0	1/2	0	0.005(1)
O(1)	0.1270(4)	0.3148(7)	−0.0396(6)	0.009(2)
O(2)	0.1318(5)	0.0269(7)	1/4	0.008(1)
O(3)	0	0.4174(11)	1/4	0.009(1)

Table 3. Selected Interatomic Distances and Bond Angles for the High-Temperature Structure of Sm_3RuO_7 and Eu_3RuO_7

	Sm_3RuO_7	Eu_3RuO_7
Ln(1)−O(1)	2.691(3) (×4)	2.688(5) (×4)
Ln(1)−O(2)	2.341(2) (×4)	2.336(3) (×4)
Ln(2)−O(1)	2.397(3) (×2)	2.396(4) (×2)
Ln(2)−O(1)	2.413(3) (×2)	2.384(3) (×2)
Ln(2)−O(2)	2.256(4)	2.254(5)
	2.264(4)	2.242(5)
Ln(2)−O(3)	2.5320(18)	2.531(3)
Ru−O(1)	1.942(3) (×4)	1.939(4) (×4)
Ru−O(3)	1.9584(17) (×2)	1.949(3) (×2)
O(1)−Ru−O(3)	85.85(13) (×4)	85.9(2) (×4)
	94.15(13) (×4)	94.1(2) (×4)
O(3)−Ru−(O3)	180.00(3)	180.00(3)
Ru−O(3)−Ru	143.5(3)	143.9(5)

monoclinic space group $P2_1/m$. They noted that the transition temperature increased with decreasing lanthanide size and reported that Sm_3RuO_7 and Eu_3RuO_7 should undergo a structural transition at ∼190 and ∼280 K, respectively;[28] however, no information concerning the low-temperature structures for these two oxides was reported.

Our ability to grow single crystals of the aforementioned compounds has enabled us to initiate an investigation to determine the structure of these low-temperature phases. To verify that we have the same material that Hinatsu reported on and to confirm that the transition temperatures for our crystals were the same as those reported for the polycrystalline powders prepared by Hinatsu et al., we performed magnetic susceptibility measurements on batches of single crystals. The data shown in Figures 4 and 5 clearly show the existence of a magnetic anomaly at ∼195 and ∼290 K for Sm_3RuO_7 and Eu_3RuO_7, respectively, in agreement with the values reported in the literature. Using this information, we performed low-temperature X-ray diffraction measurements using these single crystals.

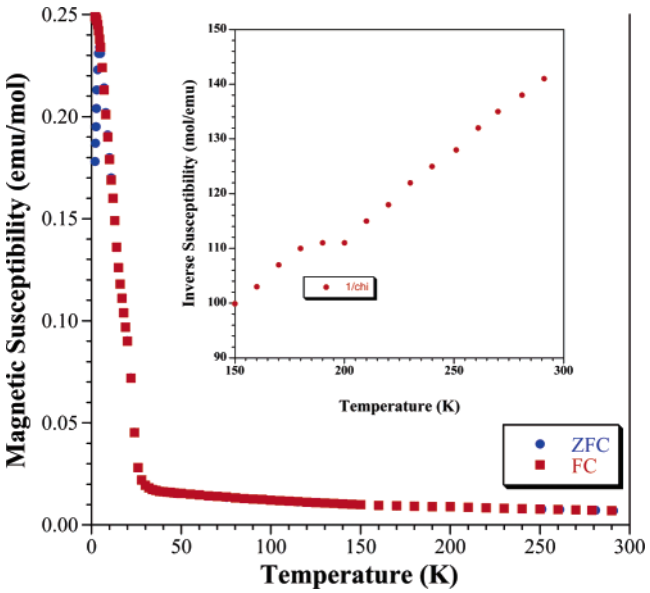

Figure 4. Temperature dependence of the susceptibility of Sm_3RuO_7 in an applied field of 10 kG. The inset is the inverse susceptibility (χ^{-1}) between 150 and 300 K showing the magnetic anomaly at ∼190 K.

Diffraction data for these crystals were collected at several temperatures and analyzed for any change in the unit cell structure. The single-crystal X-ray diffraction data demonstrate that above 190 K (Sm_3RuO_7) and 280 K (Eu_3RuO_7) these compounds exist in the expected orthorhombic fluorite-

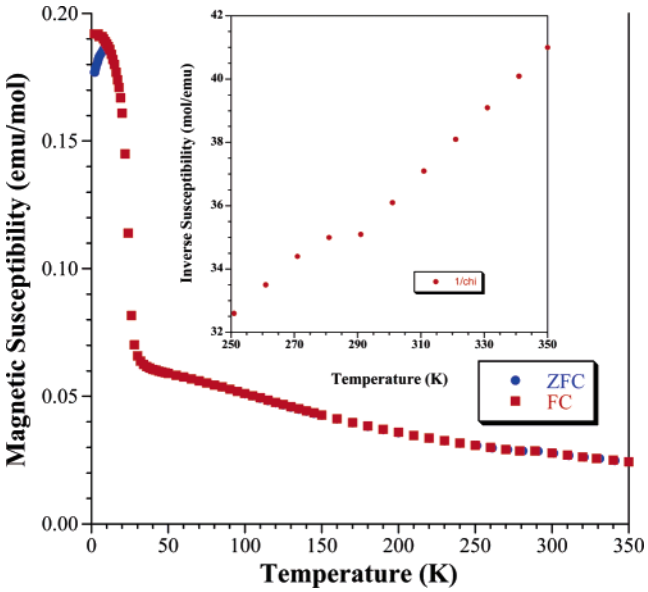

Figure 5. Temperature dependence of the susceptibility of Eu_3RuO_7 in an applied field of 10 kG. The inset is the inverse susceptibility (χ^{-1}) between 250 and 350 K showing the magnetic anomaly at ~280 K.

Table 4. Crystallographic Data and Structure Refinement for the Low-Temperature Structure of Sm_3RuO_7 and Eu_3RuO_7

empirical formula	Sm_3RuO_7	Eu_3RuO_7
fw (g/mol)	664.12	668.95
temp (K)	150(2) K	150(2) K
wavelength (Å)	0.710 73 Å	0.710 73 Å
cryst syst	orthorhombic	orthorhombic
space group	$P2_1nb$	$P2_1nb$
unit cell dimensions	a = 10.7412(3), Å α = 90°	a = 10.6783(3) Å, α = 90°
	b = 14.6661(4), Å β = 90°	b = 14.6397(4) Å, β = 90°
	c = 7.4154(2), Å γ = 90°	c = 7.3823(2) Å, γ = 90°
vol (Å^3)	1168.16(6) Å^3	1154.05(5) Å^3
Z	8	8
density (Mg/m^3)	7.552 Mg/m^3	7.700 Mg/m^3
abs coeff (mm^{-1})	32.234 mm^{-1}	34.707 mm^{-1}
reflns collected	24221	18868
indep reflns	4997 [R(int) = 0.0331]	5012 [R(int) = 0.0411]
absorption correction	semiempirical from equivalents	semiempirical from equivalents
data/restraints/params	4997/0/125	5012/0/104
GOF on F^2	1.115	1.079
final R indices [$I > 2\Sigma(I)$]	R1 = 0.0279, wR2 = 0.0561	R1 = 0.0355, wR2 = 0.0817
R indices (all data)	R1 = 0.0309, wR2 = 0.0579	R1 = 0.0393, wR2 = 0.0841
extinction coefficient	0.001 16(3)	0.002 51(6)
largest diff peak and hole (e·Å^{-3})	2.179 and −3.862	5.461 and −4.502

related structure, space group *Cmcm*. Cooling below the transition temperatures determined by the magnetic measurements leads to the appearance of numerous new reflections, illustrated in Figure 2, and a change in the space group to $P2_1nb$ for both Sm_3RuO_7 and Eu_3RuO_7. The structure transition from *Cmcm* to $P2_1nb$ involves a distortion in the trans vertex-sharing RuO_6 chains that causes a doubling of the orthorhombic *b*-axis and a concomitant reduction in the coordination environment of the Ln(1, 2) cations from 8 to 7. All crystallographic data and atomic positions for the low-temperature structures are listed in Tables 4 and 5, respectively. Selected interatomic distances and angles are listed in Table 6.

Table 5. Atomic Coordinates and Equivalent Isotropic Parameters for the Low-Temperature Structure of Sm_3RuO_7 and Eu_3RuO_7

Sm_3RuO_7				
	x	y	z	U_{eq}(Å^2)
Sm(1)	0.1872(1)	0.1363(1)	0.5022(1)	0.004(1)
Sm(2)	0.1748(1)	0.1138(1)	0.0029(1)	0.005(1)
Sm(3)	0.3978(1)	0.4742(1)	0.7641(1)	0.003(1)
Sm(4)	0.4607(1)	0.2230(1)	0.7434(1)	0.004(1)
Sm(5)	0.4517(1)	0.5303(1)	0.2521(1)	0.003(1)
Sm(6)	0.4090(1)	0.2792(1)	0.2467(1)	0.003(1)
Ru(1)	0.1806(2)	0.3748(1)	0.4981(1)	0.002(1)
Ru(2)	0.1788(2)	0.3736(1)	0.9991(1)	0.002(1)
O(1)	0.1919(9)	0.3323(4)	0.2489(5)	0.005(1)
O(2)	0.1770(9)	0.4163(4)	0.7488(5)	0.005(1)
O(3)	0.3095(5)	0.2820(4)	0.5380(7)	0.003(1)
O(4)	0.0566(5)	0.2813(4)	0.5365(7)	0.005(1)
O(5)	0.0545(5)	0.4672(4)	0.4574(7)	0.006(1)
O(6)	0.3088(5)	0.4671(4)	0.4651(7)	0.007(1)
O(7)	0.3267(5)	0.3065(4)	−0.0478(7)	0.008(1)
O(8)	0.0733(5)	0.2673(4)	−0.0399(7)	0.005(1)
O(9)	0.0256(5)	0.4394(4)	0.0451(7)	0.009(1)
O(10)	0.2838(5)	0.4823(4)	0.0415(7)	0.006(1)
O(11)	0.5488(9)	0.3661(5)	0.7569(6)	0.006(1)
O(12)	0.3088(9)	0.1169(5)	0.7618(7)	0.005(1)
O(13)	0.3125(8)	0.1439(5)	0.2373(7)	0.005(1)
O(14)	0.5478(8)	0.3942(5)	0.2370(7)	0.004(1)
Eu_3RuO_7				
	x	y	z	U_{eq}(Å^2)
Eu(1)	0.1868(1)	0.1374(1)	0.5022(1)	0.004(1)
Eu(2)	0.1731(1)	0.1125(1)	0.0030(1)	0.004(1)
Eu(3)	0.3981(1)	0.4749(1)	0.7653(1)	0.003(1)
Eu(4)	0.4611(1)	0.2239(1)	0.7424(1)	0.002(1)
Eu(5)	0.4514(1)	0.5301(1)	0.2519(1)	0.002(1)
Eu(6)	0.4104(1)	0.2789(1)	0.2458(1)	0.002(1)
Ru(1)	0.1794(2)	0.3746(1)	0.4977(1)	0.001(1)
Ru(2)	0.1776(2)	0.3733(1)	0.9988(1)	0.001(1)
O(1)	0.1841(13)	0.3326(6)	0.2492(7)	0.007(1)
O(2)	0.1685(11)	0.4174(5)	0.7482(6)	0.001(1)
O(3)	0.3099(6)	0.2823(5)	0.5382(9)	0.003(1)
O(4)	0.0558(6)	0.2808(5)	0.5359(9)	0.004(1)
O(5)	0.0549(7)	0.4681(6)	0.4567(9)	0.006(1)
O(6)	0.3083(7)	0.4677(6)	0.4650(9)	0.006(1)
O(7)	0.3296(6)	0.3085(5)	−0.0487(9)	0.006(1)
O(8)	0.0749(7)	0.2651(5)	−0.0413(9)	0.007(1)
O(9)	0.0212(6)	0.4363(5)	0.0446(9)	0.008(1)
O(10)	0.2807(6)	0.4844(5)	0.0413(9)	0.004(1)
O(11)	0.5480(10)	0.3645(7)	0.7569(8)	0.005(2)
O(12)	0.3083(9)	0.1195(6)	0.7626(8)	0.002(2)
O(13)	0.3115(9)	0.1443(6)	0.2362(8)	0.002(1)
O(14)	0.5443(10)	0.3959(6)	0.2344(9)	0.004(2)

Table 6. Average Interatomic Distances and Selected Bond Angles for the Low-Temperature Structure of Sm_3RuO_7 and Eu_3RuO_7

	Sm_3RuO_7	Eu_3RuO_7
Ln(1)−O	2.429	2.416
Ln(2)−O	2.429	2.413
Ln(3)−O	2.394	2.404
Ln(4)−O	2.406	2.376
Ln(5)−O	2.388	2.363
Ln(6)−O	2.373	2.372
Ru(1)−O	1.949	1.946
Ru(2)−O	1.947	1.949
Ru(1)−O(2)−Ru(2)	143.1(4)	141.5(4)
Ru(2)−O(1)−Ru(1)	142.5(4)	143.4(5)

The low-temperature structures are best described in the acentric primitive orthorhombic space group $P2_1nb$ with 6 independent rare earth positions, 2 unique ruthenium sites, and 14 independent oxygen atom positions. Figure 6 shows

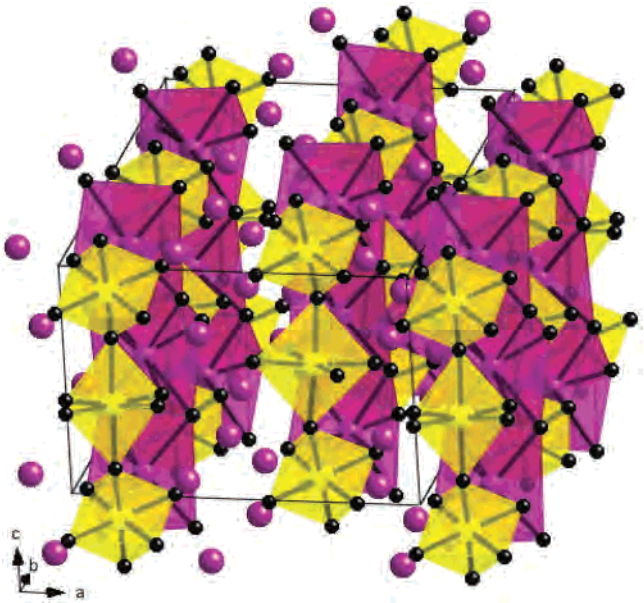

Figure 6. Crystal structure of the low-temperature $P2_1nb$ structure of Ln_3RuO_7 (Ln = Sm, Eu), emphasizing the chains of trans vertex-sharing RuO_6 octahedra (yellow) which are edge-shared to chains of Ln(1, 2)O_7 monocapped trigonal prisms (violet) along the *c*-axis. The violet spheres are the $Ln(3-6)^{3+}$ cations.

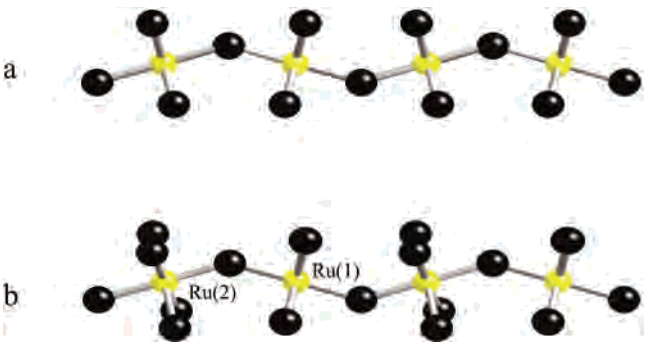

Figure 7. Views of the RuO_6 octahedral chains down the *a*-axis for (a) high-temperature structure and (b) low-temperature structure of Ln_3RuO_7 (Ln = Sm, Eu). Note the distortion of the chains in the low-temperature structure as the octahedra now tilt in both the *bc*- and *ab*-planes.

the structure of the low-temperature forms of Ln_3RuO_7 (Ln = Sm, Eu). Similar to the high-temperature phase, the structure features chains of vertex-shared RuO_6 octahedra running along the *c*-axis which now, however, are tilted in the *ab*-plane along the chain direction as well as in the *bc*-plane. This additional tilting of the chain and associated rotation of the RuO_6 octahedra, Figure 7, has the effect of reducing the coordination of the associated Ln^{3+} polyhedra [now Ln(1) and Ln(2) in $P2_1nb$] from 8 to 7, Figure 8. In the high-temperature *Cmcm* structure, the chains of trans vertex-sharing RuO_6 connect to the chains of edge-sharing Ln(1)O_8 pseudocubes via pairs of equatorial RuO_6 oxygens. In the low-temperature $P2_1nb$ structure, however, the tilting of the RuO_6 chains in the *ab*-plane and the concomitant rotation of the Ru(2)O_6 octahedra cause one of the equatorial oxygens [Ln(1)—O(9) and Ln(2)—O(7) in $P2_1nb$] to rotate away from the lanthanide cation (from ~2.69 to ~3.3 Å) while the three other oxygens [Ln(1)—O(3), O(4), O(10) and Ln(2)—O(5), O(6), O(8)] move closer. The other Ln—O

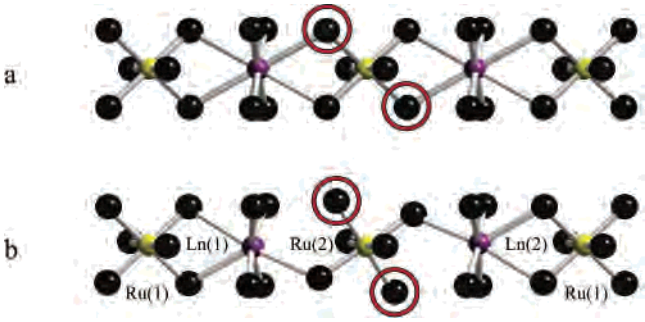

Figure 8. Coordination environments for the chains of RuO_6 octahedra and Ln(1)O_8 pseudocubes in the (a) high-temperature structure and Ru(1, 2)O_6 octahedra and Ln(1, 2)O_7-capped trigonal prisms in the (b) low-temperature structure. The analogous oxygen atoms that are in each of the structures are marked in red. In the low-temperature structure, the tilting of the Ru(2)O_6 octahedra causes the reduction in coordination in the Ln(1, 2)O_7-capped trigonal prisms, while the Ru(1)O_6 octahedra maintain their edge-sharing connectivity to the Ln(1, 2)O_7-capped trigonal prisms.

distances are not affected and remain within ~0.04 Å of their values in the *Cmcm* structure. The Ln(1)—O(9) and Ln(2)—O(7) distances of about 3.3 Å are greater than the sum of the van der Waals radii and thus reduce the coordination number from 8 to 7 (Figure 8). The coordination environment of the lanthanide is now best described as a capped trigonal prism. It should be noted that the Ru(1)O_6 octahedra maintain their edge-sharing connectivity with both Ln(1) and Ln(2), and it is only the rotation of the Ru(2)O_6 octahedra that causes the oxygen to move out of the Ln(1, 2) coordination sphere. The Ru—O distances, on the other hand, are not affected by the structural distortion, and the average Ru—O distances are 1.948 Å for both Sm_3RuO_7 and Eu_3RuO_7 (Table 6). In the low-temperature structure, the RuO_6 chains still connect to the rare earth chains to form sheets, Figure 9, between which the remaining rare earth cations exist in four crystallographically unique sites, Ln(3)—Ln(6), as distorted pentagonal bipyramids. The Ru—Ln—O slabs are more distorted in the low-temperature structure, which can be clearly seen in Figure 9, which shows the view down the *c*-axis.

The structural transition is associated with a slight change in the magnetic susceptibility, as shown in Figures 4 and 5. The upward shift in the inverse susceptibility is consistent with an increase in the antiferromagnetic coupling in both Sm_3RuO_7 and Eu_3RuO_7. The cause for this change is most likely due to the small decrease in the intrachain Ru—Ru separation of ca. 0.1 Å (average) in the low-temperature structures of both compounds. As these changes are small, it is not surprising that the effect on the magnetism, also, is very minor.

As the transition temperature increases with decreasing rare earth size, one can speculate that the transition is stress-induced and indirectly a function of the lattice contraction on cooling. In the Ln_3RuO_7 series, the known transition temperatures range from 130 K in Nd_3RuO_7 to 382 K in Gd_3RuO_7. Similar transitions have been observed in the analogous iridates, in which they range from 261 K in Pr_3IrO_7 to 485 K in Eu_3IrO_7. It is not clear at this point whether all the low-temperature structures distort either to the monoclinic $P2_1/m$ or the orthorhombic $P2_1nb$ structures or

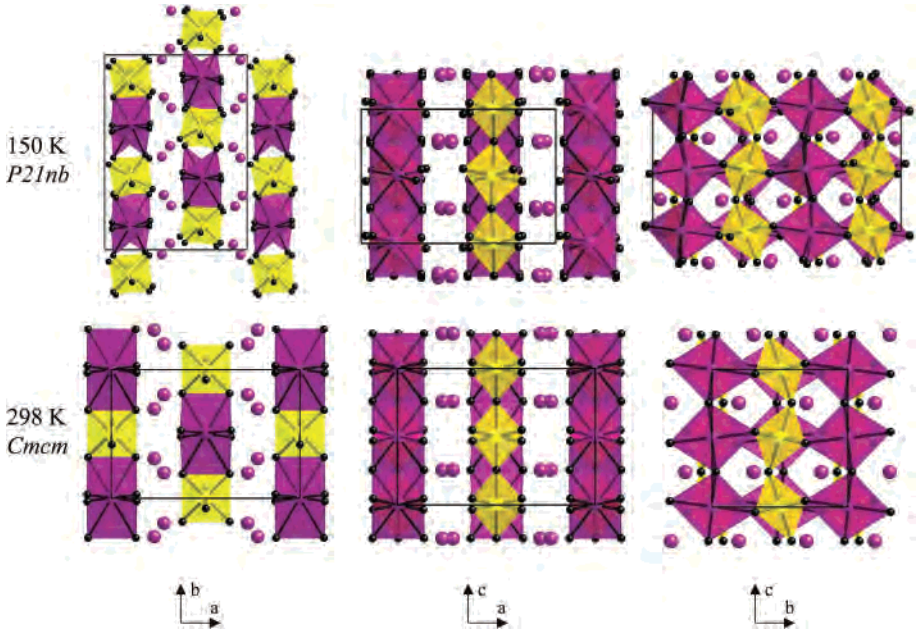

Figure 9. Comparative views of the high- and low-temperature structures as viewed down each of the crystallographic axes.

whether other structure types exist. To answer this question, we are working on the crystal growth and single-crystal structure determination of the remaining ruthenates and iridates of this family.

Summary

The two fluorite-related ruthenates of the stoichiometry Ln_3RuO_7 (Ln = Sm, Eu) were synthesized in single-crystal form and structurally characterized. The growth of these oxides from molten hydroxide fluxes further establishes these melts as a successful solvent system for the preparation of oxide structures containing both lanthanides and platinum group metals. A temperature-induced structural transition results in a loss of lattice centering, a doubling of the *b*-axis, and a reduction in the coordination environment of one of the lanthanides from 8- to 7-fold. For the first time, the low-temperature structure of this structure type has been completely characterized by single-crystal X-ray diffraction. Further investigations are currently underway to prepare single crystals of isostructural compounds containing other platinum group metals.

Acknowledgment. Financial support for this research was provided by the National Science Foundation through Grant DMR:0134156.

Supporting Information Available: Additional structural and crystallographic data. This material is available free of charge via the Internet at http://pubs.acs.org.

IC049700L